Appl Phys A 2268

Holographic recording mechanisms of gratings in indium oxide films using 325 nm Helium-Cadmium laser irradiation

C. Grivas [(1)]*, S. Mailis [(1)], R.W. Eason [(1)], E. Tzamali [(2)], N. A. Vainos [(3)]

[(1)] Optoelectronics Research Centre (O.R.C.), University of Southampton, Southampton SO17 1BJ, United Kingdom

[(2)] Foundation for Technology and Research-Hellas (FO.R.T.H.), Institute of Computer Science (I.C.S), P.O.Box 1527, 71110 Heraklion, Greece

[(3)] National Hellenic Research Foundation (NHRF), Theoretical and Physical Chemistry Institute, Engineered Photonic Media Lab, 48 Vassileos Constantinou Avenue, 11635 Athens, Greece

PACS: 42.40.Eq; 42.70.Ln; 81.15.Fg

* Corresponding author.

E-mail:chg@orc.soton ac.uk, Tel.: ++44 (0)2380 593139, Fax: ++44 (0) 2380 593142

Abstract: UV (325 nm) holographic recording of gratings in indium oxide films fabricated by reactive pulsed laser deposition has been investigated as a function of growth temperature, oxygen pressure and angle of incidence of the plasma plume on the substrate. The influence of the ambient environment (air or vacuum) and the film temperature during recording has also been studied. Large steady state refractive index changes up to $6x10^{-3}$ were observed in layers grown at an oblique angle of 75°. About 77% of the magnitude of these changes residues after thermal annealing and is attributed to UV induced permanent structural rearrangements. In contrast, refractive index changes in films grown at normal incidence were smaller in magnitude and completely reversible.

1.Introduction

Indium oxide (InO_x) is one of the most representative broad band semiconducting oxides (E_g=3.75 eV [1]) having characteristics that make it attractive for applications such as transparent conducting coatings, flat panel displays, solar cells and switching devices [1,2]. The electrical conductivity of InO_x films is related to their stoichiometry; stoichiometric In_2O_3 is an insulator while in non-stoichiometric form exhibits high conductivity, high reflectivity in the IR region and high optical transparency in the visible region. Amorphous InO_x, (E_g=3 eV [1]), has also received considerable attention for fundamental research as the only amorphous semiconductor in which the Fermi level can be shifted through the energy gap into the conduction band [3] leading to ambipolar transport. Due to this property the material has been extensively investigated to understand transport properties near the metal-insulator transition. The electrical conductivity of InO_x is affected by the concentration of oxygen vacancies, which act as doubly ionized donors and can contribute two electrons to the conduction band. Another approach to increase further the number of carriers is doping with elements which have at least four valence electrons. Much work has been done with tin doped InO_x [4-7] and recently multicomponent oxides have received much attention [8, 9].

Holographic information storage continues to receive much attention due to its capability of providing three-dimensional storage and retrieval in the same volume using a variety of multiplexing methods. The main concept of this technique involves as a first step recording of a large number of holograms in a common volume of photosensitive material with further spatial multiplexing to increase the required storage capacity. The main impediment in the development of holographic memories is the lack of materials that can simultaneously meet requirements such as long-term storage, fast response as well as capability of non-destructive readout of the holographically stored information. Photorefractive crystals are the most widely used materials so far for applications in the areas of information storage and dynamic information processing because they offer advantages

such as high-density storage and readout rate [10]. InO_x layers exhibit photosensitivity in the UV spectral region and are promising therefore candidates for high resolution holographic applications. On UV irradiation, both amorphous and polycrystalline InO_x films were reported to undergo photoreduction or oxidation, exhibiting reversible transitions between conducting and insulating states [11, 12]. Changes in conductivity were attributed to alteration of the film stoichiometry and particularly the concentration of oxygen vacancies. Holographic recording of gratings has already been demonstrated in films grown by reactive D.C. magnetron sputtering [13, 14, 15] and pulsed laser deposition (PLD) [16].

Here we report an investigation of the UV holographic recording of gratings in InO_x films grown by PLD. Our motivation for this was to gain insight into the recording mechanism with respect to the morphological characteristics, the stoichiometry and the electrical properties of the deposited layers. These parameters are interrelated and strongly influenced by the growth conditions. Furthermore, it would be interesting to develop films with optimized properties for applications in the areas of holographic information storage and information processing through control of the deposition parameters.

In this paper the recording dynamics in InO_x films were studied as a function of various growth parameters including growth temperature, oxygen pressure and plume direction during deposition. In particular, the dependencies of induced refractive index change and decay of diffraction efficiency, which are linked to the response time and long-term storage respectively, have drawn our attention. Additionally, we have investigated the correlation between electrical conductivity and diffraction efficiency by simultaneous monitoring of their temporal dynamics as well as the grating response as a function of film temperature during recording. Based on these results we distinguish two types of UV-induced optical changes depending on whether the initial state can be re-establish after thermal annealing treatment. In films deposited at normal plume incidence on the substrate reversible

changes were observed, in sharp contrast to the ones deposited at a 75° oblique angle where the effects were irreversible. We suggest two different structural modification mechanisms responsible for grating recording in each class of films.

2. Experimental details

Depositions were performed in a stainless steel vacuum chamber, which was evacuated down to a base pressure of 5×10^{-4} Pa. InO_x films were grown by pulsed laser ablation of a pure indium target in a background oxygen atmosphere ranging from 0.5 to 50 Pa. Irradiation was provided by a KrF excimer laser (Lambda Physik, LPX 200, 248 nm, pulse duration ~20 ns) operated at 10 Hz, and focused to an energy density of 2 J/cm^2 on the target. Films were deposited on Corning glass substrates positioned at a distance of 7 cm away from the target material. All films employed for the investigation had a thickness of ≈250 nm. To localize the substrate heating and to prevent contamination through desorption from the walls of the reaction chamber a 100 W CO_2 laser (Synrad 57-1-28W) was used as a heating source [17]. This heating technique has already been implemented successfully in PLD [18, 19]. To achieve spatial homogenization of the CO_2 laser beam a copper four-sided reflecting light pipe was positioned just before the 10mm×10mm substrate. To achieve homogeneous temperature distribution over the substrate area, the substrate was attached to a boron nitride plate and both were fixed on a ceramic holder. The growth temperature was measured using a platinum-platinum-rhodium thermocouple built in the boron nitride plate in direct contact with the substrate.

********** FIGURE 1 **********

The experimental set up employed for holographic recording of gratings in InO_x films was similar to that described in [16]. Briefly, recording was performed using a He-Cd laser operating at the wavelength of 325 nm (3.8 eV>E_g). A dielectric beam splitter was employed to divide the laser light into two mutually coherent symmetrical beams each having an irradiance of 40 mW/cm^2. The two beams were made to interfere with each other on the InO_x

film at an angle of 20° producing an interference pattern with fringe spacing Λ=936 nm. Monitoring of the recording dynamics was performed by means of a 6.5 mW He-Ne laser beam (λ=633 nm), which was at normal incidence to the InO_x film. Three different diffraction orders of the He-Ne beam were observed. The wavelength of the reading beam was outside the absorption band of the film [16] in order to avoid destructive read out of the grating. The evolution of the holographic recording was investigated by measuring the first order diffraction efficiency. For recordings performed at low temperatures films were mounted in a cryostat (Fig. 1).

********** FIGURE 2 **********

3. Results and Discussion

3.1 Morphological characteristics

The influence of the deposition parameters on the microstructural characteristics of the InO_x layers was studied by means of Transmission Electron Microscopy (TEM). To avoid any structural transformation such as crystallization due to possible electron beam induced heating, low current densities were employed. Figure 2 shows high-resolution electron micrographs (HREM) of InO_x films grown at an oxygen pressure of 5.5 Pa and substrate temperatures of 25°C (room temperature, RT) (Fig. 2a), and 600°C (Fig. 2b). X-Ray Diffraction (XRD) analysis has shown [16] that films grown at RT contained amorphous indium oxide and a few metallic indium phases. The dark spots in Fig. 2a correspond to the indium clusters, which are embedded in the amorphous matrix. The film is composed of fine crystallites of about 5 nm in size. As the temperature increased, films showed crystallization with larger grain size, which at 600°C were from 30 to 70 nm in size indicating a decrease in film porosity. The stoichiometry of the InO_x films was investigated by Rutherford Backscattering Spectroscopy (RBS). Figure 3 shows RBS spectra of films grown at an oxygen pressure of 5.5 Pa and RT (Fig. 3a) as well as 600°C (Fig. 3b). The points in these figures represent the experimental data and the solid lines the simulation to the data by

assuming particular composition and thickness for the deposited layers. A good agreement between the simulated and the measured spectra was obtained by assuming a 380 nm thick $In_2O_{2.7}$ layer (Fig. 3a) and a 320 nm thick In_2O_3 film (Fig. 3b) for films grown at RT and 600°C respectively. The discrepancy at the In peak in Fig. 3b is thought to be due to diffusion of the deposited layer into the substrate.

********** FIGURE 3 **********

3.2 Recording characteristics and electrical properties

Figure 4 shows recording dynamics of gratings in InO_x films fabricated by varying parameters such as growth temperature, oxygen pressure, film temperature during recording as well as angle of incidence of the plasma plume on the substrate. The curves shown in Fig 4a and b correspond to films grown at RT and an oxygen pressure $P(O_2)$ of 5.5 and 8 Pa respectively. Figure 4c shows the diffraction efficiency evolution of a grating in a film grown at 600°C and a $P(O_2)$ of 5.5 Pa. The curve in Fig. 4d was obtained by maintaining the film temperature at 80°K during recording. Figure 4e shows the recording dynamics in a film grown at an oxygen angle of 75°. Both the films in Figs. 4d and e were fabricated at RT and a $P(O_2)$ of 8 and 5.5 Pa respectively. Holographic recording of gratings in PLD grown InO_x films shows a dynamic behaviour. At time $t \cong 0$, we observe a sharp increase in the diffraction efficiency followed by a systematic decrease and stabilisation to a steady lower value. Once a stable value had been established the recording was stopped inducing a decay of the recorded grating to a steady level, which is indicated with dotted lines (Fig 4). The dotted lines are extrapolations of the evolution of the diffraction efficiency and were derived by fitting single exponential decay curves to the experimental data. The difference between the initial (dashed lines) and the final steady state level corresponds to the optical memory effect. Its intensity depends on growth and recording conditions and is higher for obliquely grown films (Fig.4e) and low recording temperatures (Fig. 4d) whereas, it decreases with increasing oxygen pressure (Fig. 4b) and growth temperature (Fig. 4c).

********** FIGURE 4 **********

To elucidate the effect of the fabrication conditions on the temporal behavior of the recorded gratings, the dark decay time constant and the change in refractive index were studied as functions of oxygen pressure and growth temperature. The dark decay time constants were derived by single exponential decay curves fitted to the experimental curves. The investigation was performed in films grown at RT, at normal and oblique (75°) angles of plume incidence on the substrate. As shown in Fig. 5a for normal incidence the decay time increases steeply with increasing oxygen pressure between 3 and 5.5 Pa and shows a sharp maximum at 5.5 Pa. However, with further increasing oxygen pressure it decreases substantially. For settings lower than 3 Pa recording was not possible due to the metallic nature of the fabricated layers. The value of dark decay time with growth temperature is shown in Fig. 5b, where data points correspond to films grown at a $P(O_2)$ of 5.5 Pa. For the normal incidence deposition, the maximum decay time constant (310 sec) was measured in films grown at RT. With increasing growth temperature it decreases down to a value of 2 sec for stoichiometric films, grown at 600°C. Obliquely grown films, show systematically higher decay time constants while their dependence on oxygen pressure and growth temperature is similar to those of the normal incidence deposited ones.

********** FIGURE 5 **********

The change in the refractive index of absolute value $|\Delta n|$ as a function of oxygen pressure and growth temperature is shown in Figures 6a and b respectively. $|\Delta n|$ was derived from measurements of the diffraction efficiency (η) via the thin grating diffraction equation [20]:

$$\eta = J_1^2 (2\pi d \Delta n / \lambda), \qquad (1)$$

where J_1 corresponds to cylindrical Bessel function, which for small arguments reduces to:

$$\eta \cong (\pi d \Delta n / \lambda)^2, \qquad (2)$$

where d stands for the film thickness, and λ is the recording wavelength. The dependencies of $|\Delta n|$ on oxygen pressure and growth temperature are similar to those observed for the dark

decay time constant as seen from Fig. 6. $|\Delta n|$ increases with increasing oxygen pressure for values between 3 and 5.5 Pa and again reaches a maximum at 5.5 Pa. At higher values ($P(O_2)$>5.5 Pa), $|\Delta n|$ decreases as the oxygen pressure increases. Additionally, $|\Delta n|$ shows a maximum in films grown at RT and decreases with increasing growth temperature. Absolute values were used for the refractive index change since its sign cannot be determined from measurements of the diffraction efficiency. As observed in other photosensitive materials such as lead germanate [21, 22] and germanium doped silica [23] the growth parameters are highly likely to have a substantial influence on the sign.

********** FIGURE 6 **********

To study the influence of oxygen pressure and substrate growth temperature on electrical conductivity, InO_x films were grown on glass substrates, which had two thermally evaporated NiCr electrodes on their surface. The spacing between the electrodes was smaller than the spot size of the UV writing beams. By applying the two-point method this configuration enabled us to monitor any change in conductivity when the area between the electrodes was exposed to the UV writing beams. Simultaneously we were able to monitor the development of the diffraction efficiency during the recording procedure. Figure 7 shows the simultaneous development of the diffraction efficiency and the conductivity. Measurements were performed in a film grown at normal incidence, RT and an oxygen pressure of 12 Pa. Immediately after the onset of the irradiation a sharp increase in both the diffraction efficiency and the conductivity is observed. These increases are attributed to the UV laser induced excitation of charge carriers from the valence band and the impurity levels within the gap into the extended states. Within a few seconds they reach saturation and after the UV beam is blocked they both decrease exponentially. Fitting with single exponential decay curves gives similar decay time constants, being 50 and 47 sec for the conductivity and the diffraction efficiency respectively, thereby suggesting that these effects are interrelated. The decay of the electrical conductivity to a non-zero steady state level, indicates that depending on growth conditions the UV irradiation can induce either an increase in film

conductivity or a transition from the insulating into a conducting state.

********** FIGURE 7 **********

Figures 8a and b show the change in electrical conductivity as a function of growth temperature and oxygen pressure respectively. This change is given by the ratio $\mathcal{R} = (C_{max}-C_{min})/(C_{max})$, where (C_{max}) and (C_{min}) are the maximum and the minimum conductivity values as measured during and before the UV-irradiation of the film respectively. We observe that for oxygen pressures between 2 and 5.5 Pa $\mathcal{R}$ shows a steep increase and then drops in the region between 6 and 30 Pa. At low settings ($P(O_2)<2$ Pa) conductivity remains essentially unchanged due to the metallic nature of the grown films. On the other hand, at high pressures ($P(O_2)>30$ Pa) the observed photoconductivity effect is very weak due to the decreased concentration of potential charge carriers (oxygen vacancies). As shown in Fig. 8b, $\mathcal{R}$ is maximum for films grown at RT and decreases with increasing growth temperature. Interestingly, the dynamics of the change in refractive index as in Fig. 5 and in conductivity (Fig. 8) upon UV irradiation are similar with both the growth temperature and the oxygen pressure providing further evidence for the absorptive nature of the recorded gratings.

********** FIGURE 8 **********

3.3 *Recording mechanism in films grown at normal incidence*

Dynamic changes in the refractive index of layers grown at normal incidence may arise by local changes in the absorption coefficient through the Kramers-Kronig relation. Such changes result from UV induced transitions between configurational states in defect sites, which in turn are attributed to bond rearrangements through electronic excitations. Due to the low intensity laser irradiation employed for the recording, any structural changes resulting from a laser-induced increase in temperature of the layers are not likely to occur. On irradiation with the 325 nm He-Cd laser band gap irradiation carriers (primarily electrons from the oxygen vacancies, and oxygen ions) are excited to the conduction band and then within picoseconds relax to the bottom levels where they may undergo trapping by defect sites to form defect centers. Finally the electronic relaxation terminates with their radiative or

nonradiative recombination. Major sources of electron scattering, which might contribute to the relaxation process in the InO_x films are grain boundaries, phonons as well as impurities such as O^{2-} ions. The recombination process can induce some transient lattice distortions at defect sites with a consequent impact on the precise atomic locations. We suggest that such structural rearrangements at defect points such as oxygen vacancies are the principal cause of the light induced index change. Similar structural modifications resulting from electronic excitations at strained bonds or impurities have been reported for glasses [24-26]. In InO_x, oxygen 2p and indium 5s electrons are at the top of the valence and the bottom of the conduction band respectively [1], hence, the optical absorption process can involve electron transfer from oxygen to indium according to the reaction:

$$O^{2-} + In^{3+} \rightarrow O^{-} + In^{2+} \qquad (3)$$

The disordered structure of the InO_x films and particularly the presence of oxygen vacancies allow for O^- and O^{2-} ion mobility. As a consequence O^- ions can move towards neighboring O^{2-}, leading to formation of weak covalent bonds. Also stronger bonds between neighboring O^{2-} ions can form [27].

During UV irradiation a light saturated state is gradually established, which is characterized by a dynamic equilibrium between the thermal transition process to the conduction band and the thermal relaxation to a configuration of lower energy. When the irradiation is interrupted a new dynamic equilibrium will be established. As a consequence the transient bond configuration of the self-trapped holes may either relax to the original state or become metastable. This will induce a decay response of the diffraction efficiency with a decay time constant which is affected by the speed of the bond relaxation and depends on film properties and consequently on fabrication conditions. As already mentioned, the magnitude of the steady state level to which the diffraction efficiency decays, indicates the intensity of the optical memory effect in the film. A non-zero steady state level is associated with the photodarkening or the photobleaching effect. Photodarkening corresponds to a red

shift in the optical absorption edge of the film induced by band gap irradiation [24, 25, 28], which leads to an increase in refractive index. For absorption gratings the film growth parameters can determine the sign of $|\Delta n|$ by influencing the width of the band gap. If the width exceeds the photon energy, the sub-bandgap irradiation will induce a blue shift in the optical absorption (known as photobleaching), and subsequently negative refractive index changes. Since the photon energy of the recording beams (3.8 eV) exceeds E_g and the gratings are absorptive in nature the observed refractive index changes in InO_x films are attributed to photodarkening. As shown in Fig. 4a and c $|\Delta n|$ is larger in films grown at RT and low oxygen pressure. As revealed by the XRD [16] and RBS analysis (Fig. 3a) these conditions lead to fabrication of amorphous films with more oxygen vacancies (10% oxygen deficiency with respect to the stoichiometric In_2O_3) and subsequently higher number of carriers. In sharp contrast to crystals, these amorphous disordered states have a higher degree of metastability, meaning that they can exist in many different configurations having local energy minima, which differ little and are separated by low energy barriers. Therefore, the energy of a photon is large enough to cause a transition to a different configuration. This explains the decrease in the intensity of the photodarkening effect in InO_x films with increasing growth temperature and subsequently with improving crystallinity. The thermal stability of the recorded gratings depends on the barrier height, which separates the metastable from the initial state. The photo-optical changes observed in the layers grown at normal incidence are reversible via annealing at an elevated temperature (100°C).

However, other proposed mechanisms such as photoinduced stress changes [29] may also contribute to the observed refractive index changes. Stress changes are facilitated by internal mechanical stresses arising during film deposition and the flexibility of the film lattice. According to this scheme the sinusoidal light distribution developed on the InO_x film by the HeCd laser beams induces changes in the internal mechanical stress distribution with the same periodicity as that of the light intensity pattern. The modulated mechanical stress

causes a displacement of atoms adjacent to vacancies without breaking the chemical bonds. This displacement enables a transitional motion of unfilled sites such as pores, voids and vacancies from the holographic grating maxima to the minima or vice versa leading to density modulation and subsequently to changes in the absorption and refractive indices.

********** FIGURE 9 **********

To investigate the effect of film temperature during recording on the evolution of diffraction efficiency the experimental set up shown in Fig. 1 was used. As shown in Fig. 4d at low recording temperatures the initial rise in the diffraction efficiency is substantially less than at RT (Fig. 4b). This is attributed to the increase in the width of the band gap with decreasing temperature and consequently to the smaller fraction of charge carriers which is excited to the conduction band. Additionally, the decay is also substantially less at low temperatures. With decreasing film temperature from RT to 80°K an increase in the decay time constant from 133 to 457 sec, and in the steady state level of $|\Delta n|$ from 1.4×10^{-4} to 2.6×10^{-4} was observed. This is because the low film temperature suppresses the thermal relaxation from the final structural state to the metastable or to the initial state. Figure 9 shows the dynamics of recording in a film grown at RT and an oxygen pressure of 10 Pa. The two curves correspond to recordings performed while the film was held in ambient air and in a background vacuum of 0.1 Pa respectively. The recording in vacuum shows longer decay time constant (174 sec) and larger $|\Delta n|$ (1.6×10^{-4}) than in air, where the corresponding values are 109 sec and 1.2×10^{-4}. This may result from a UV induced photoreduction induced in the InO_x films irradiated under vacuum or argon atmosphere as reported in [11]. Photoreduction may either occur in the bulk of the film [27] or result from outdiffusion of oxygen to an extent that is affected by the porosity of the structure [30]. As a consequence, the number of oxygen vacancies increases, providing additional free electrons, which in turn leads to an improvement of the recording performance.

3.4 Recording in obliquely deposited layers

As shown in Fig. 6 the 75° obliquely deposited films exhibit larger photo-induced refractive index changes than the films grown at normal incidence. However, this effect is evident only for growth temperatures up to 300°C (Fig. 6b). At higher temperatures the angle of plume incidence on the substrate has no influence on the recording dynamics. Thermal annealing at 100°C of films grown at low temperatures (≤300°C) can only partly reverse the photo-optical changes. Thus, in a film grown at RT and a $P(O_2)$ of 5.5 Pa $|\Delta n|$ was reduced from $6x10^{-3}$ to $4.6x10^{-3}$ (a 23% reduction). The reversible part is very close to the refractive index changes induced in the film grown at normal incidence under the same conditions ($|\Delta n| = 1.2x10^{-3}$). It seems that for the oblique angle deposition, changes in refractive index primarily result from a modification of the physical structure of the film and to a smaller extent from a change in the absorption index. The difference in nature of the photo-induced structural changes is associated with the particular microstructural characteristics that arise from the deposition geometry. In general, amorphous films can exist in different structural states depending on their preparation method. In fabrication with evaporation techniques such as thermal evaporation or pulsed laser ablation large deviations of the deposition direction from the normal to the 75° oblique angle deposition of these InO_x films, can lead to formation of highly porous and low density films with columnar morphology due to geometrical shadowing. This effect has already been reported for glasses [31 and references therein] and various metal oxides [32, 33]. Voided or intercolumnar regions allow for easy transport of ions across the film, which is of great importance for the dynamics of holographic recording of gratings. The extent of the voided network strongly depends on deposition parameters and particularly on growth temperature. Growth on cool substrates may lead to formation of films with a highly disordered nature and loose material packing [25, 31-33].

As suggested by Fritzsche [25] the basic mechanism behind both the reversible and the irreversible optical/structural changes in glasses and amorphous materials is common and involves modifications of atomic configurations and positions that result from non radiative

recombinations via transient self-trapped excitons. Reversibility is possible only when the initial and final structures belong to states that can be reached by changing the temperature, light intensity, or pressure. On the other hand, irreversible structural changes are defined by material preparation conditions and are substantially different from the annealed state. With reference to the above, the common origin of the structural modifications responsible for the recording in the normal and the obliquely deposited InO_x films is the self-trapping of holes in week O-O bonds after the charge transfer process from O^{2-} to In^{3+}. A possible mechanism, which can explain the further irreversible structural modifications in the obliquely deposited films and the accompanying refractive index changes is the crystallization of the indium phase. Coherent and incoherent UV irradiation of InO_x films has been recently reported to be effective in the crystallization of indium and indium oxide respectively [34]. Crystallization of indium phases involves charge transfer from O^{2-} to In^{3+} and then successive migration of indium atoms in the amorphous matrix and formation of crystalline clusters. The structural particularities of the obliquely deposited layers would have favored this process for two reasons. Firstly, indium atoms can migrate quite easily in the voided network of the structure, which allows for photo-induced diffusion of atoms over an interatomic distance [25]. Secondly, the indium particles embedded in the amorphous matrix, can serve as defect sites for formation of crystalline indium clusters.

Another possible mechanism, which could explain the irreversible structural changes is the collapse of the voided or columnar structure upon the UV irradiation. Such an effect has been reported as being responsible for similar effects in Ge-chalcogenide films [31]. The intensity of the irreversible effects depends strongly on the extent of the voided network, and this explains their appearance in the obliquely deposited layers grown at low temperatures. With increasing growth temperature the grain size becomes larger leading to a decrease in the void volume as well as the spacing between any columnar structures. Due to the overall film densification the photo-optical changes become electronic in nature as in the normal

incidence grown films. This is in very good agreement with the recording features in films grown at high temperatures (≥300°C), where very few persisting density inhomogeneities are expected to exist.

4. Conclusions

In summary, holographically recorded gratings in pulsed laser deposited InO_x films show a dynamic behaviour and depending on growth and recording conditions large differences in their photosensitivity were observed. The key factor, which determines the recording mechanism and the nature of the accompanying structural rearrangements is the deposition geometry. Thus, obliquely deposited films show steady state refractive index changes up to $6x10^{-3}$, of which magnitude a 77% remained after thermal annealing. In sharp contrast, for films deposited at normal plume incidence the photo-optical changes are smaller in magnitude and completely reversible. UV-induced optical changes in obliquely deposited layers are attributed to permanent structural rearrangements favored by their highly disordered structure. On the other hand, simultaneous observation in normal incidence films of the dynamics of recording and conductivity has demonstrated that the feasibility of recording and its dynamics are associated with changes in the conductive state of the film under UV irradiation. Finally, recordings in films maintained at low temperature (80°K) or in vacuum can also lead to a substantial increase in the magnitude of the UV induced optical changes.

Acknowledgements: *Part of this research was performed at the Foundation for Research and Technology–Hellas (FORTH), Institute of Electronic Structure and Laser (IESL), Heraklion, Greece. The authors are grateful to Dr. Peter Chandler for the RBS analysis.*

REFERENCES

(1) I. Hamberg and C.G. Cranqvist: J. Appl. Phys. **60**, 19, (1986)

(2) J.R. Bellingham, W.A. Phillips, C.J. Adkins: J.Phys.: Condens. Mater. **2**, 6207, (1990)

(3) N.Tsuda, K.Nasu, A. Yanase, K. Siratori: *Electronic Conduction in Oxides,*Springer Series in Solid State Sciences 94, (Springer-Verlag, Berlin, 1991)

(4) J.P. Zheng, H.S. Kwok: Appl. Phys. Lett., **63,** 1, (1993)

(5) M. Rotmannn, K.H. Hencker: J.Phys.: Appl. Phys. **28**, 1448, (1995)

(6) M. Higushi, S. Uekusa, R. Nakano, K. Yokogawa: J. Appl. Phys. **74**, 6710, (1993)

(7) R.B.H. Tahar, T. Ban, Y. Ohya, Y. Takahashi: J. Appl. Phys. **144,** 183, (1997)

(8) T. Minami, T. Miyata, T. Yamamoto: J. Vac. Sci. Technol. A **17,** 1822, (1999)

(9) T. Minami: J. Vac. Sci. Technol. A **17,** 1765, (1999)

(10) J.H. Hong, I. McMichael, T.Y. Chang, W. Christian, E. G. Paek: Opt. Eng., **34,** 2193, (1995)

(11) H. Fritzsche, B. Pashmakov, B. Clafin: *Solar Energy Materials and Solar Cells* **383,** 1994, (1993)

(12) C. Xirouhaki, G. Kyriakidis, T.F. Pedersen H. Fritzsche: J. Appl. Phys., **79**, 1, (1996)

(13) S. Mailis, L. Boutsikaris, N.A. Vainos, C. Xirouhaki, G. Vasiliou, N. Garawal, G. Kyriakidis: Appl. Phys. Lett. **69,** 2459, (1996)

(14) K. Moschovis, E. Gagaoudakis, E. Hatzitheodoridis, G. Kiriakidis, S. Mailis, E. Tzamali, N.A. Vainos, H. Fritzsche: J. Appl. Phys. A **66,** 651, (1998)

(15) S. Pissadakis, S. Mailis, L. Reekie, J.S. Wilkinson, R.W. Eason, N.A. Vainos, K. Moschovis, G. Kiriakidis: Appl. Phys. A **69**, 333, (1999)

(16) C. Grivas, D.S. Gill, S. Mailis, L. Boutsikaris, N.A. Vainos: Appl. Phys. A, **66,** 201, (1998)

(17) S. J. Barrington, R. W. Eason: Rev. Sci. Inst. **71**, 4223, (2000)

(18) A.A. Anderson, R.W. Eason, M. Jelinek, C. Grivas, D. Lane K. Rodgers, L.M.B. Hickey, C. Fotakis: Thin Solid Films **300**, 68, (1997)

(19) A.A. Anderson, C.L. Bonner D.P. Shepard, R.W. Eason, C. Grivas D.S. Gill, N.A. Vainos: Opt. Commun. **144,** 183, (1997)

(20) H.J. Eichler, P. Guenther, D.W. Pohl: *Laser-induced Dynamic Gratings* (Springer, Berlin, Heidelberg 1986)

(21) S. Mailis, A.A. Anderson, S.J. Barrington, W.S. Brocklesby, R. Greef, H.N. Rutt, R.W. Eason, N.A. Vainos, C. Grivas: Opt. Let. **23**, 697, (1998)

(22) S. Mailis, L. Reekie, S. Pissadakis, S.J. Barrington, R.W. Eason, N.A. Vainos, C. Grivas: Appl. Phys A, **69,** S671, (1999)

(23) M.V. Bazylenko, D. Moss, J. Canning: Opt. Lett. **23,** 697, (1998)

(24) G. Pfeifer, M.A. Paesler, S.C. Agarwal: J. Non-Cryst. Solids **130,** 111, (1991)

(25) H. Fritzsche: Philos. Mag. B **68**, 561, (1993)

(26) K. Tanaka: J. Appl. Phys., **65**, 2042, (1989)

(27) B. Pashmakov, B. Clafin, H. Fritzsche: Solid State Commun. **86,** 619, (1993)

(28) A.E. Owen, A.P. Firth, P.J.S. Ewen: Philos. Mag. B **52,** 347, (1985)

(29) A. Ozols, O. Salminen, M. Reinfelde: J.Appl. Phys. **75,** 3326, (1994)

(30) B. Clafin, H. Fritzsche: *J. Electron. Mat.* **25,** 1772, (1996)

(31) S. Rajagopalan, K.S. Harshavardhan, L.K. Malhotra, K.L. Chopra: J. Non-Cryst. Solids **50**, 29, (1982)

(32) T. Motohiro, Y. Taga: Appl. Opt. **28,** 2466, (1989)

(33) C.G. Granqvist: Appl. Phys. A, **57**, 19, (1993)

(34) H. Imai, A. Tominaga, H. Hirashima, M. Toki, N. Asakuma: J. Appl. Phys. **85,** 203, (1999)

FIGURE CAPTIONS

Figure 1. Experimental set up employed for holographic recording of gratings at low temperatures in pulsed laser deposited InO_x films. R_1 and R_2 correspond to He-Cd writing beams, P to the He-Ne probe beam, and $S_{\pm 1}$ to the first order diffraction of the probe beam. PM and ID stand for the power meter head and the iris diaphragm respectively.

Figure 2. Transmission electron micrographs of InO_x films grown at an oxygen pressure of 5.5 Pa and a substrate temperature of **(a)** 25°C (room temperature) and **(b)** 600°C.

Figure 3. Rutherford backscattering spectra of InO_x films grown at an oxygen pressure of 5.5 Pa and substrate temperature of **(a)** 25°C and **(b)** 600°C respectively. The data points correspond to experimental results and the solid lines represent the theoretical fit by assuming a stoichiometry of ratio **(a)** $In_2O_{2.7}$ and **(b)** In_2O_3 respectively.

Figure 4. Recording dynamics in InO_x films grown at a substrate temperature and an oxygen pressure which vary from **a** to **e** as follows: **(a)** 25°C and 5.5 Pa, **(b)** 25°C and 8 Pa, **(c)** 600°C and 5.5 Pa, **(d)** 25°C and 8 Pa, **(e)** 25°C and 5.5 Pa. All curves correspond to films grown at normal plume incidence on the substrate apart from **(e)** where the incidence angle was 75°. In **(d)** the film was held at a temperature of 80°K during recording. Y-axis values [arbitrary units (A.U.)] are proportional to the diffraction efficiency. The arrows indicate the end of the irradiation with the UV writing beams.

Figure 5. Dark decay time of gratings in InO_x films as a function of **(a)** oxygen pressure for films grown at room temperature and **(b)** growth temperature for films fabricated at an oxygen pressure of $P(O_2)$=5.5 Pa. Data points correspond to films grown at: (•) normal angle, (□) a 75° oblique angle.

Figure 6. Absolute values of the UV-induced refractive index change in InO_x films as a function of **(a)** oxygen pressure for films grown at room temperature and **(b)** growth temperature for films fabricated at an oxygen pressure of 5.5 Pa. Data points correspond to films grown at: (•) normal incidence, (□) 75° oblique incidence, (◊) 75° oblique incidence and after annealing at 100°C.

Figure 7. Simultaneous evolution of **(a)** diffraction efficiency of a grating and **(b)** electrical conductivity in a InO_x film grown at room temperature and an oxygen pressure of 12 Pa. The arrows indicate the end of the irradiation with the UV writing beams.

Figure 8. UV induced change in electrical conductivity of InO_x films as a function of **(a)** oxygen pressure for films fabricated at room temperature and **(b)** growth temperature for films grown at an oxygen pressure of 5.5 Pa.

Figure 9. Evolution of diffraction efficiency in a InO_x film, which was held in **(a)** ambient air and **(b)** a background vacuum of 10^{-1} Pa. The film was fabricated at room temperature and at an oxygen pressure of 10 Pa.

FIGURE 1: C. Grivas et al. " *Holographic recording...*"

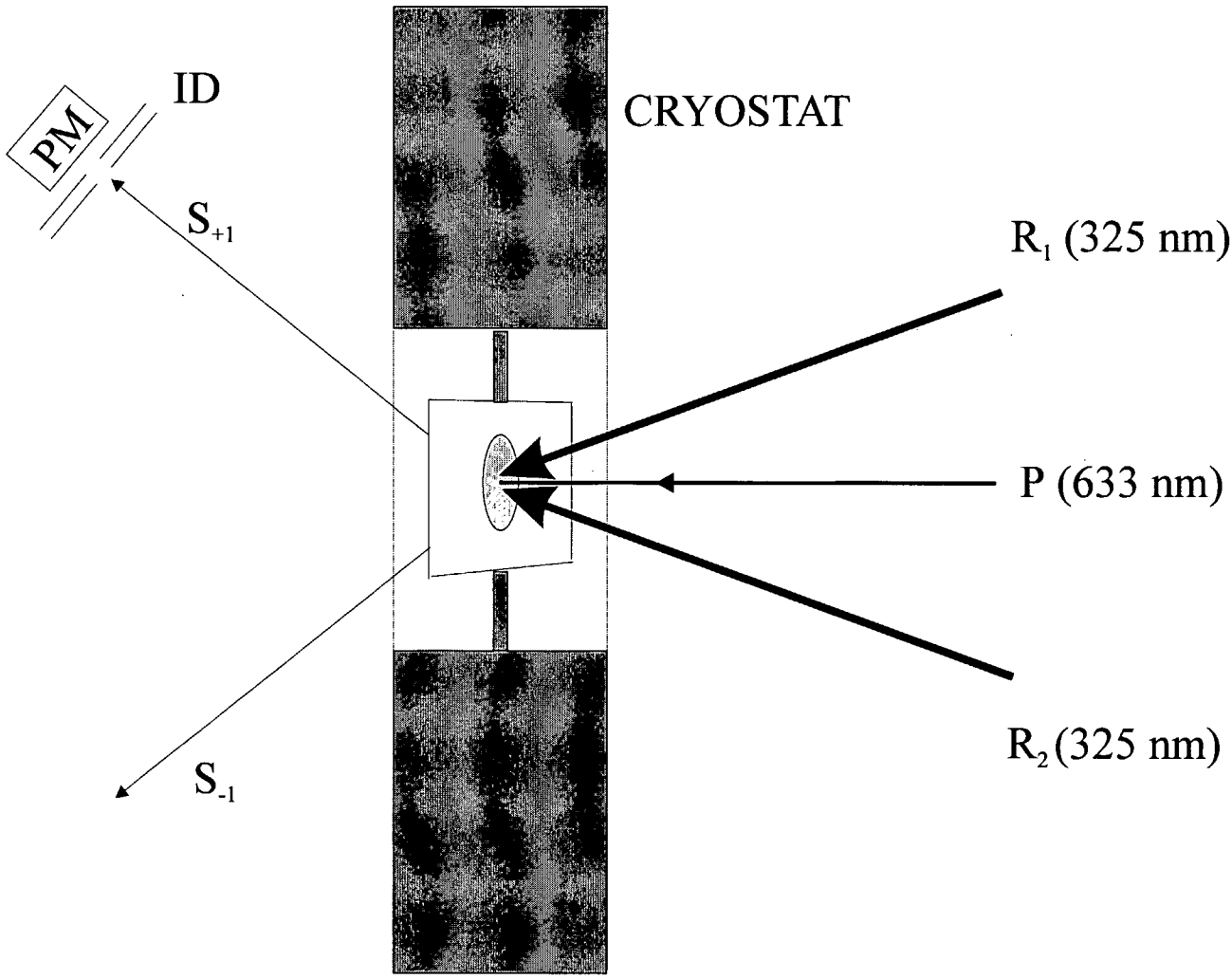

FIGURE 2: C. Grivas et al. "*Holographic recording....*"

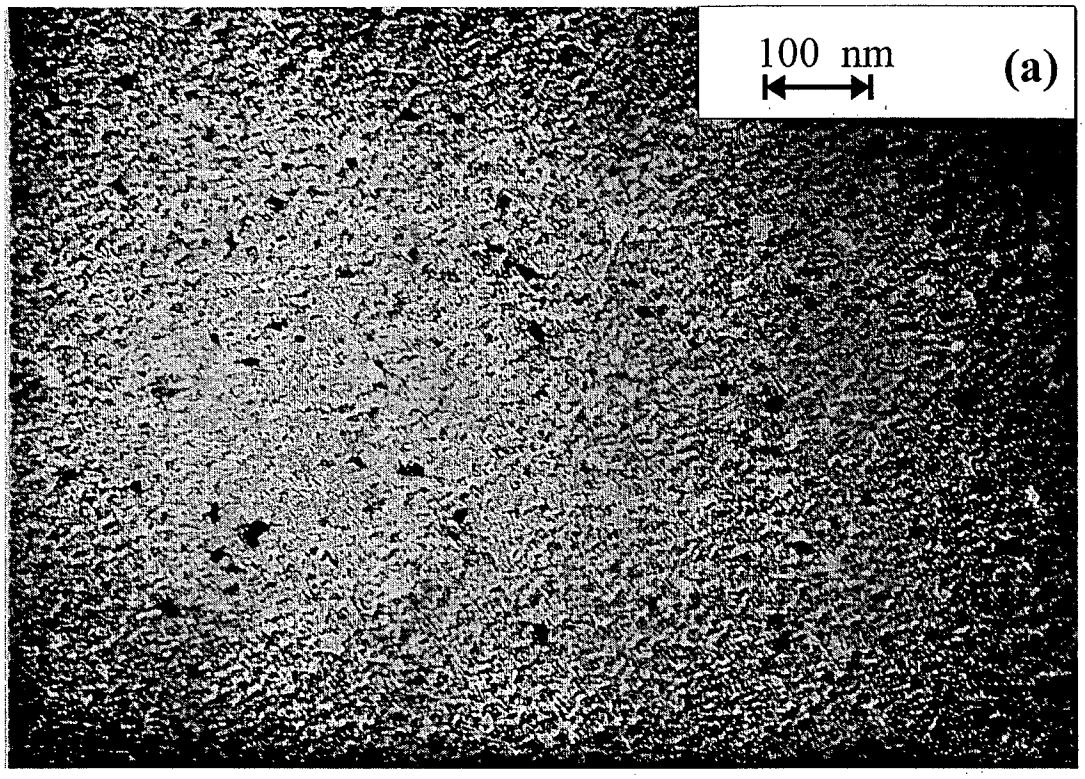

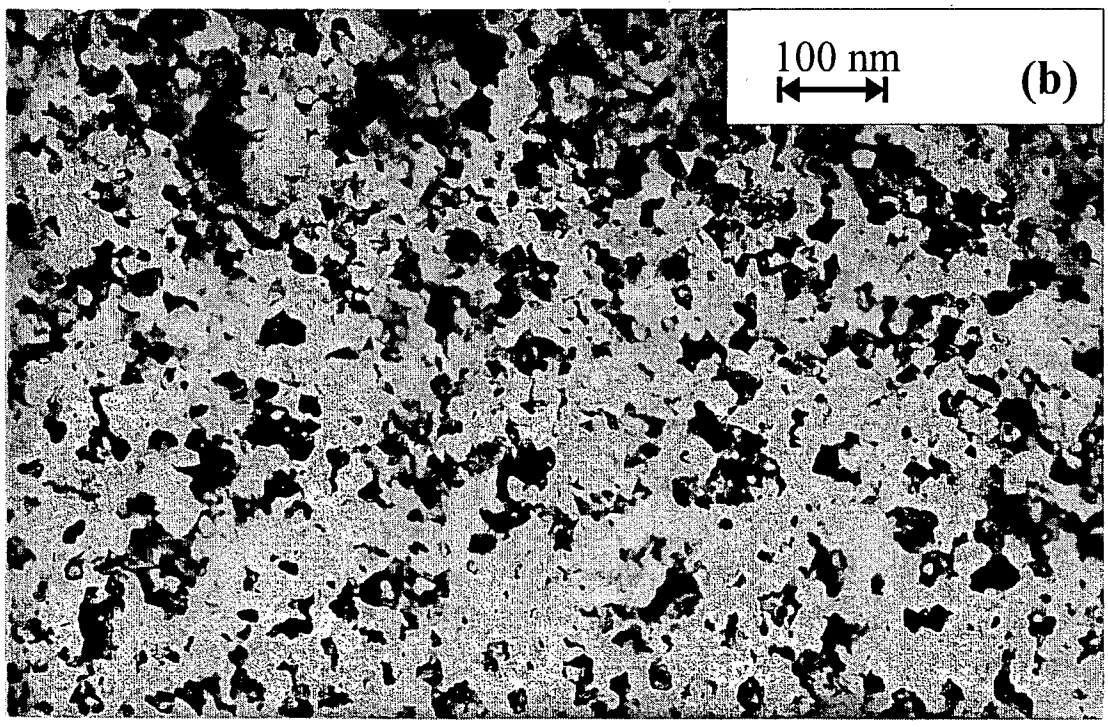

FIGURE 3: C. Grivas et al. "*Holographic recording....*"

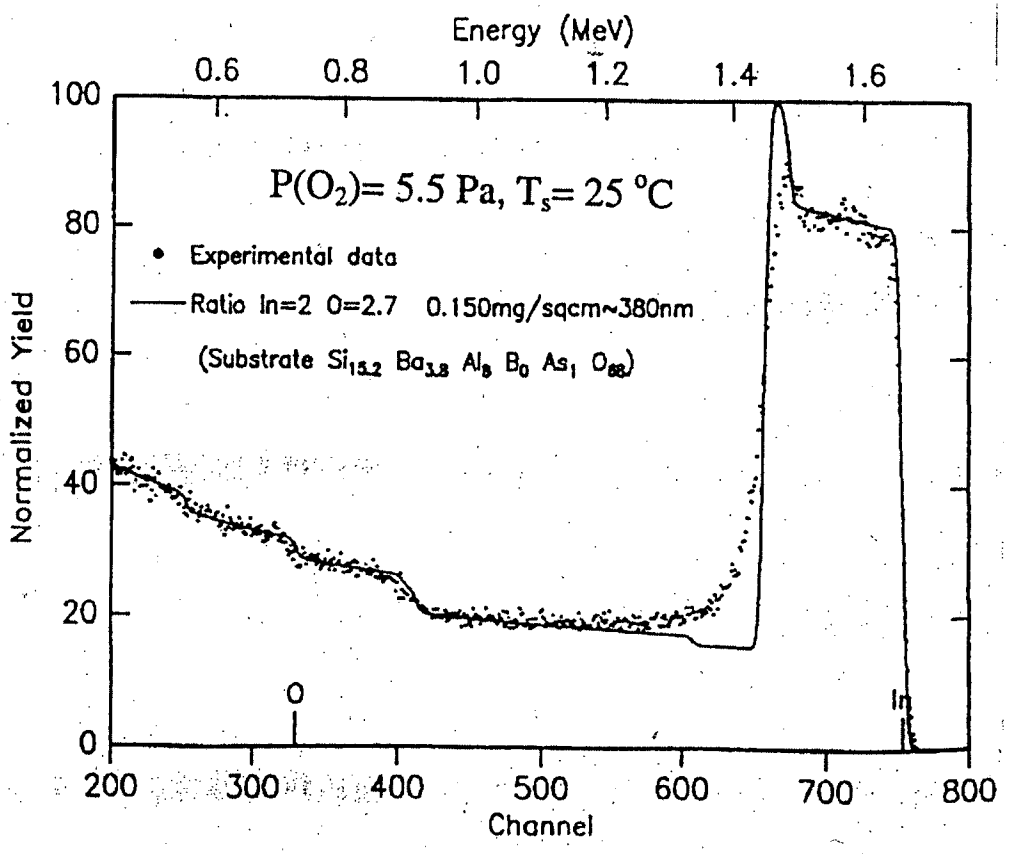

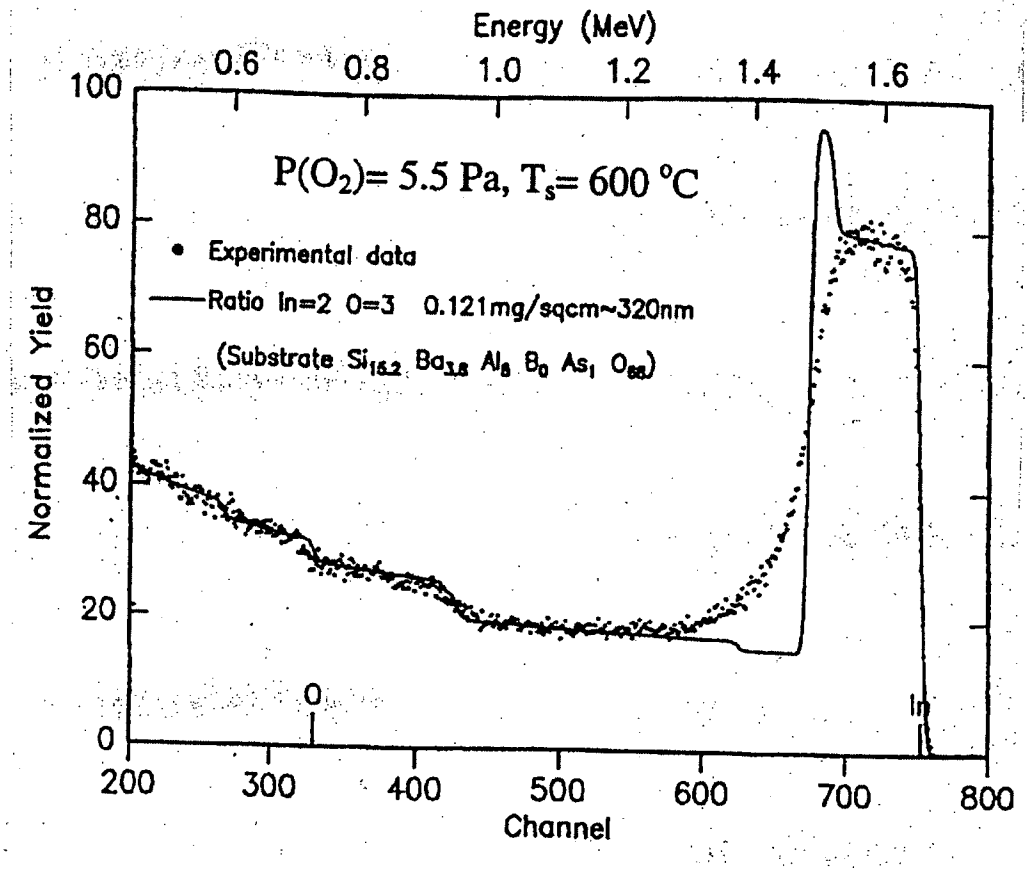

FIGURE 4: C. Grivas et al. "*Holographic recording...*"

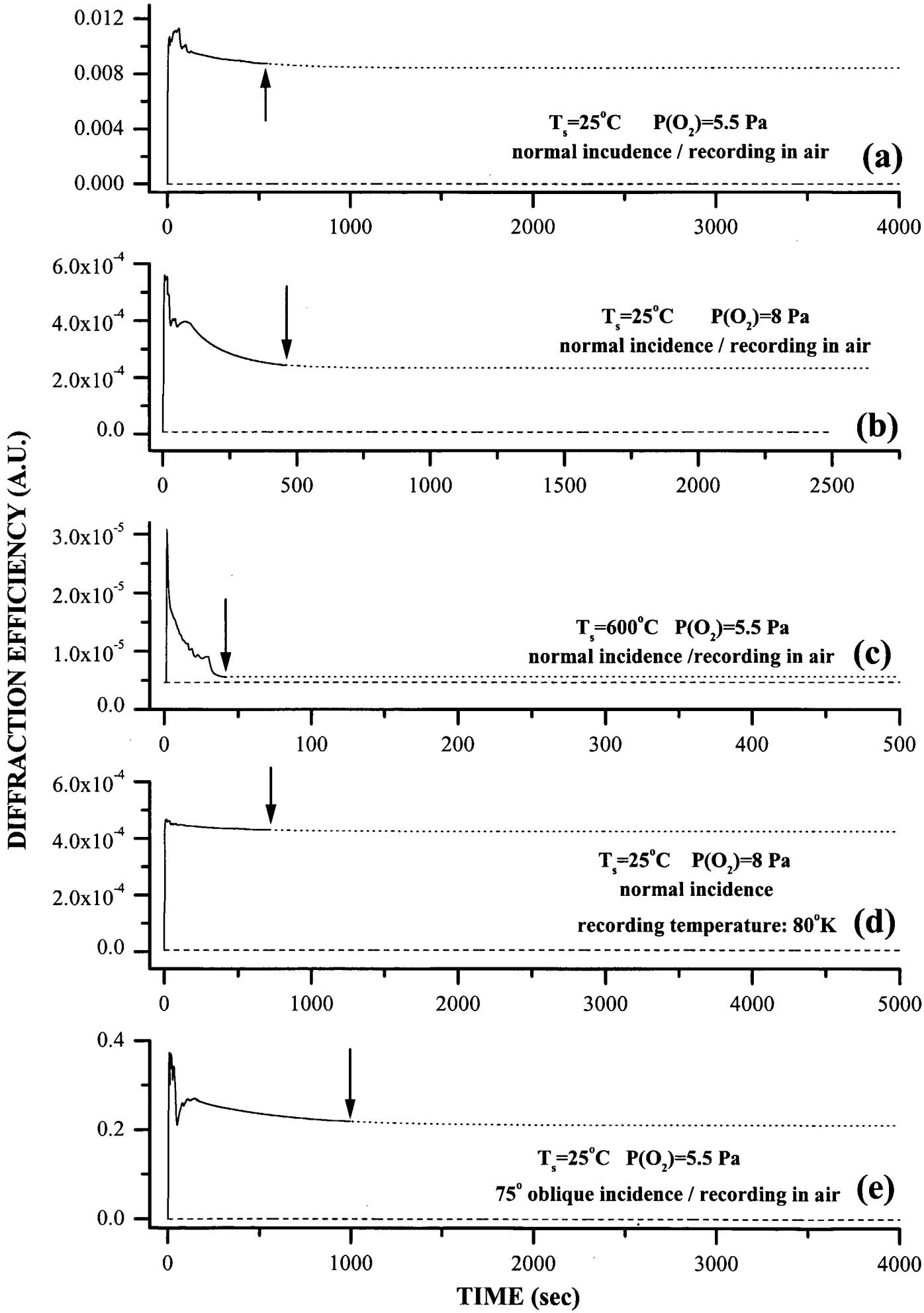

FIGURE 5: C. Grivas et al. "*Holographic recording...*"

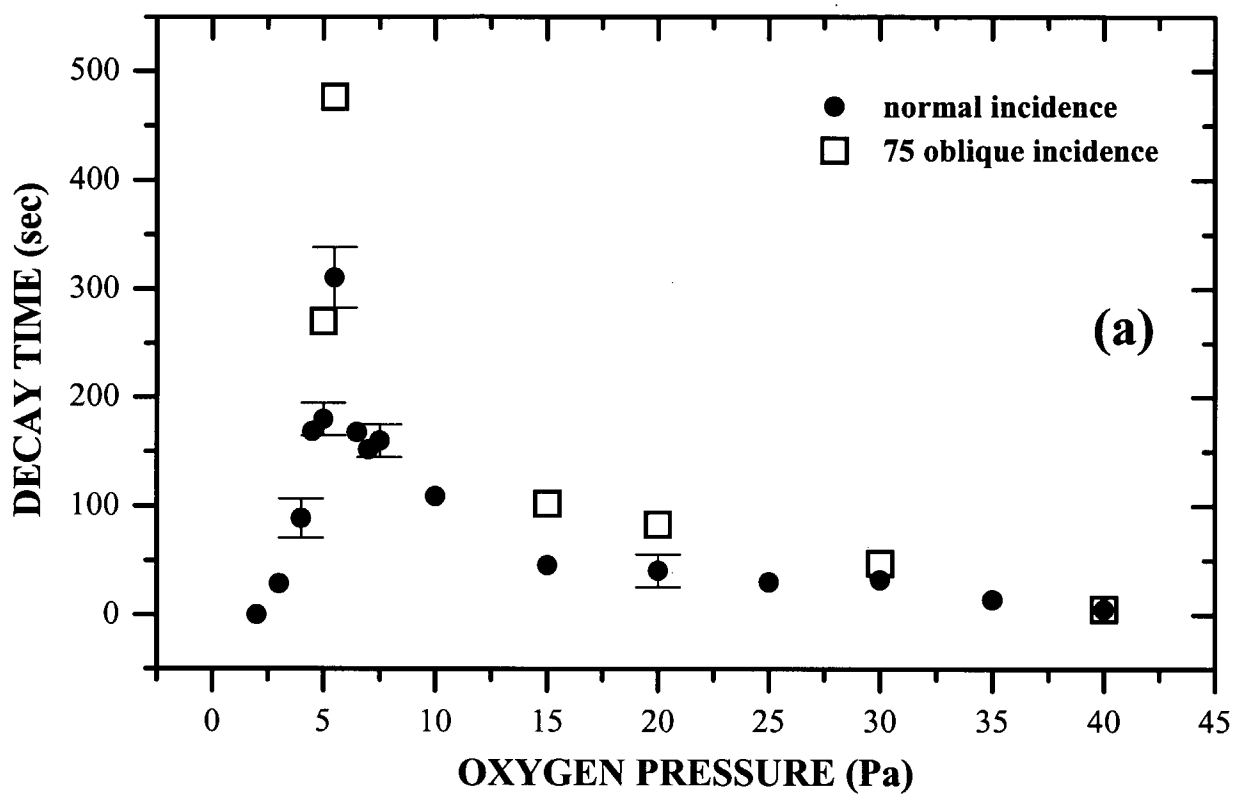

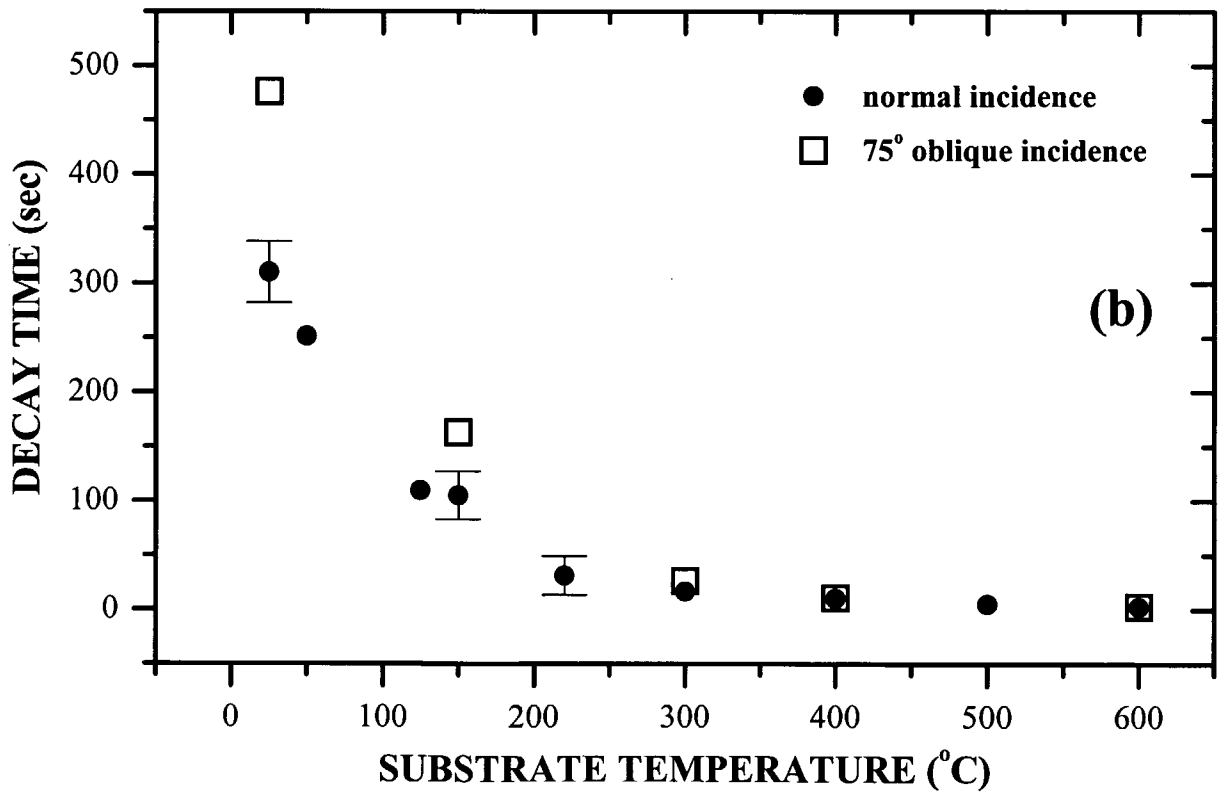

FIGURE 6: C. Grivas et al. "*Holographic recording....*"

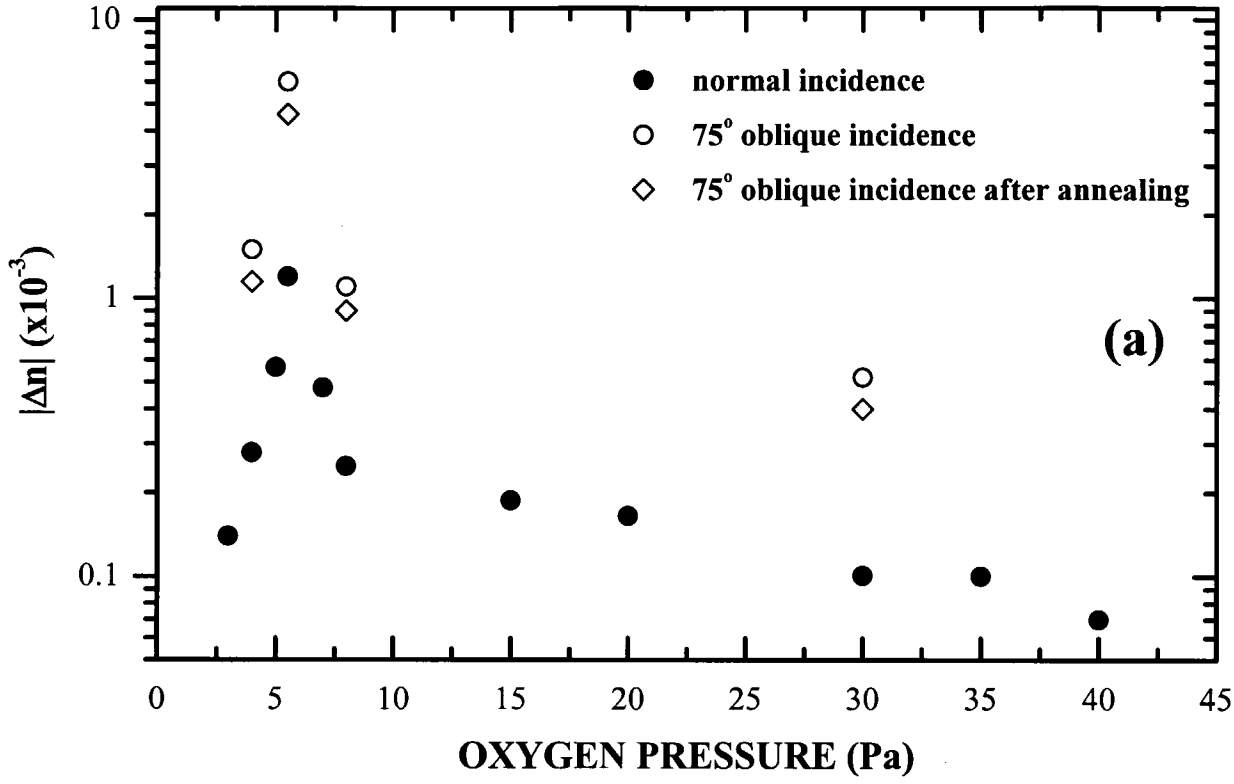

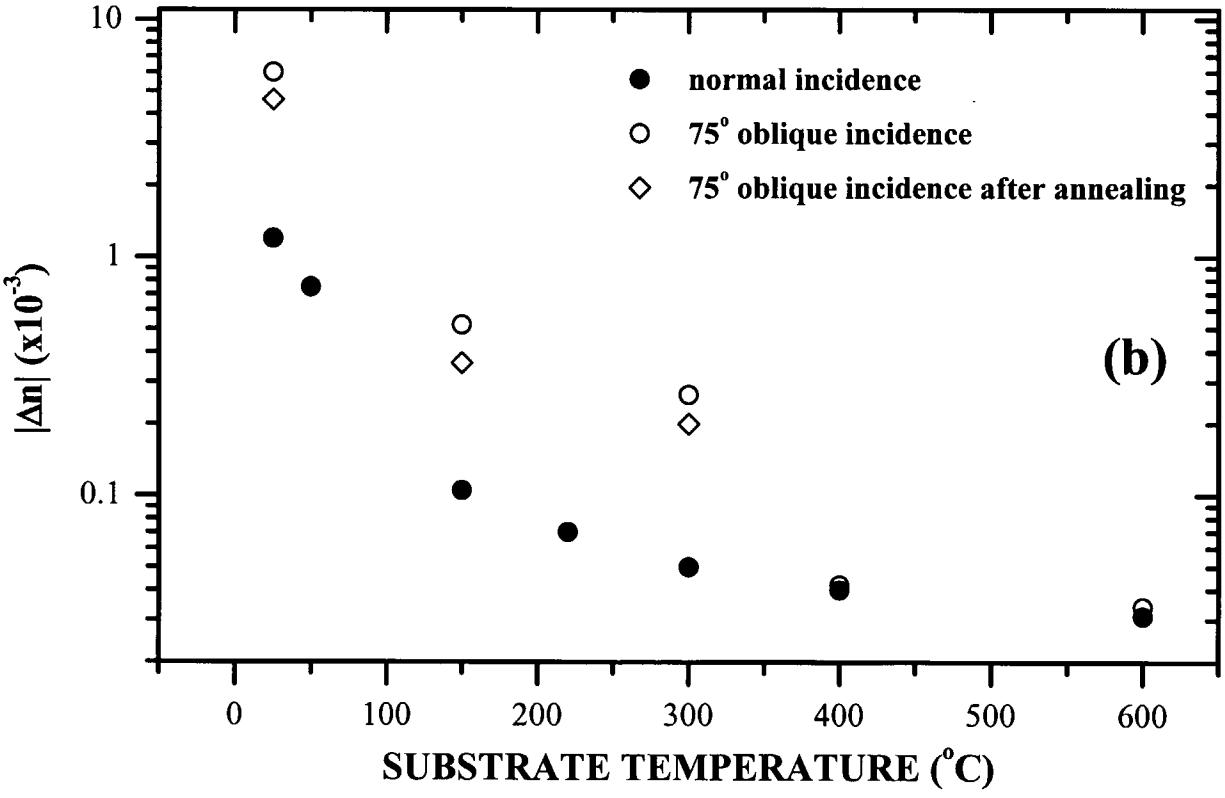

FIGURE 7: C. Grivas et al. "Holographic recording..."

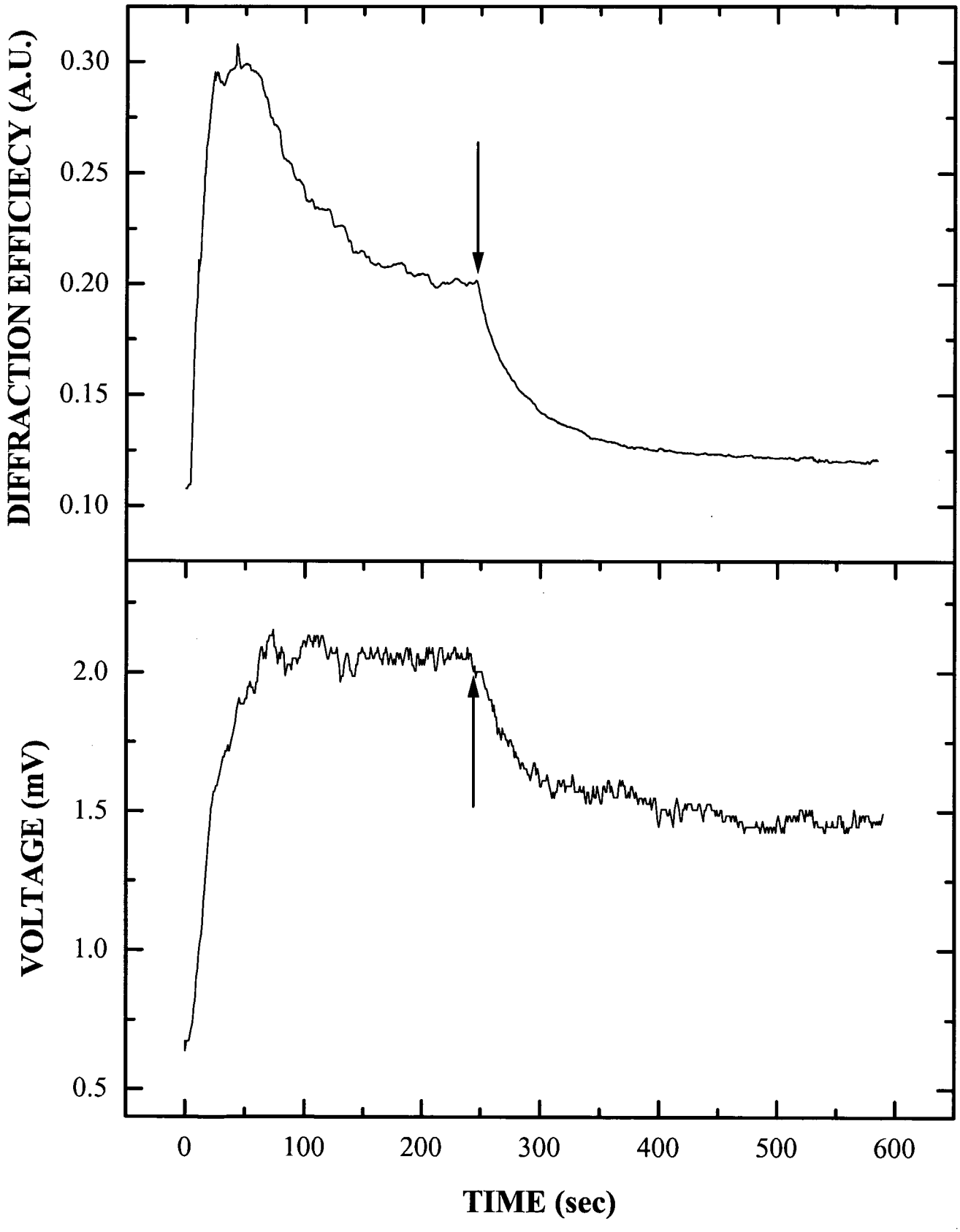

FIGURE 8: C. Grivas et al. "*Holographic recording ..*"

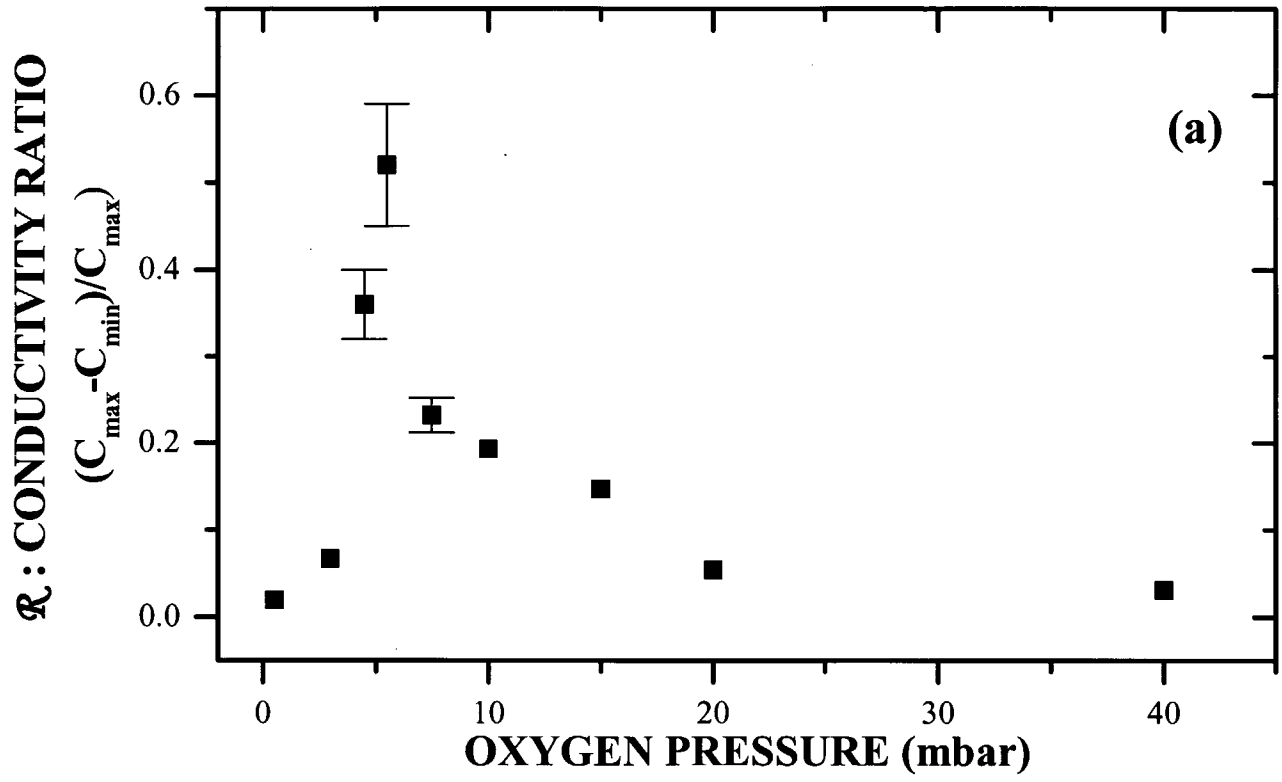

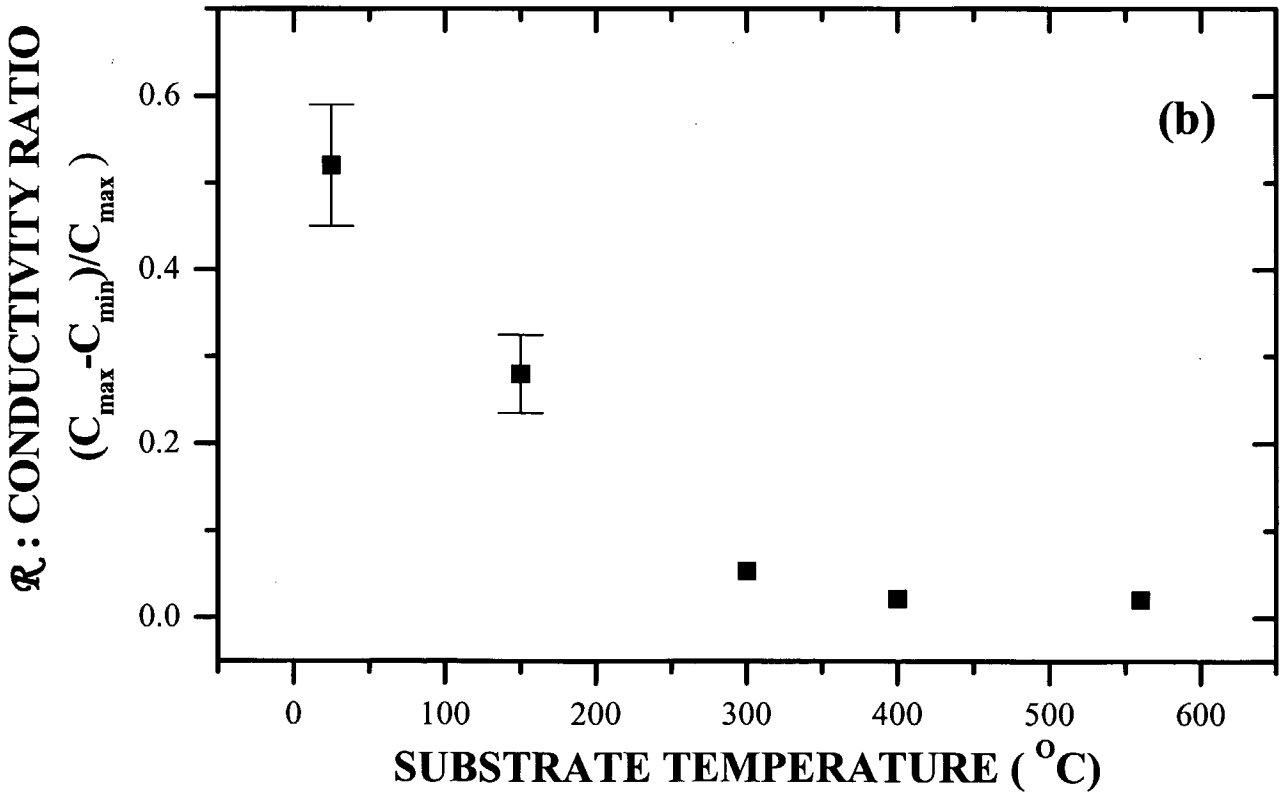

FIGURE 9: C. Grivas et al. "*Holographic recording...*"